IL NUOVO CIMENTO **45 C** (2022) 88
DOI 10.1393/ncc/i2022-22088-5

COMMUNICATIONS: SIF Congress 2021

Characterization of the ENEA extreme ultraviolet radiation discharge produced plasma source, by using diamond detectors developed at the University of Rome "Tor Vergata"

L. MEZI(*)(**)

ENEA, Fusion and Technologies for Nuclear Safety Department, Plasma Studies Division, Plasma Applications and Interdisciplinary Experiments Laboratory - Via E. Fermi 45, 00044 Frascati (Rome) Italy

received 18 February 2022

Summary. — After a brief introduction, including a summing up of the main characteristics of the Extreme Ultraviolet (EUV) radiation, we describe the ENEA Discharge Produced Plasma (DPP) EUV source. The DPP emits 100-ns duration EUV pulses, in the $\lambda = 10$–18 nm wavelength spectral range. The in-band energy per pulse is about 30 mJ/sr at 10 Hz repetition rate. In addition to the already performed characterizations, we recently exploited high purity monocrystalline diamond detectors developed at the Department of Industrial Engineering of the University of Rome "Tor Vergata". The configuration of the electrodes of the used devices was the interdigitated one, particularly suitable for fast measurements. Thanks to the rapid temporal response of these detectors, the fast peaks of EUV emission (7–8 ns FWHM), superimposed on the main pulses, have been characterized much better than when using silicon PIN diodes. These rapid emission peaks occur at the maximum heating and radial compression of the plasma column. Finally, by using the DPP source, a useful characterization and calibration of the diamond detectors has been obtained in the $\lambda = 10$–18 nm range, by comparison with a reference absolute PIN diode.

1. – Introduction

This work derives from a scientific collaboration between ENEA, that is responsible for the Extreme Ultraviolet (EUV) radiation source operation, and the Department of

(*) On behalf of the scientific collaboration between the ENEA group (S. Bollanti, F. Bombarda, F. Flora and L. Mezi) and the University of Rome "Tor Vergata" group (S. Cesaroni, M. Marinelli, S. Palomba, C. Verona and G. Verona Rinati).
(**) E-mail: luca.mezi@enea.it

Industrial Engineering of the University of Rome "Tor Vergata" (URTV), that is responsible for the development and fabrication of the diamond detectors [1].

EUV radiation (total band photon energy $h\nu = 20$–$284\,\mathrm{eV}$, wavelength $\lambda \simeq 4.4$–$62\,\mathrm{nm}$) is gaining considerable scientific and technological interest for its numerous applications concerning material treatments, fusion plasma diagnostics and microelectronic fabrications [2]. In particular, EUV radiation can be efficiently utilized both to modify the chemical structure of many materials [3,4] and to influence optical properties of various photonic materials [5,6]. Moreover, the combination of EUV short wavelengths with the availability of high reflectivity ($\geq$70% around $\lambda = 13$–$15\,\mathrm{nm}$) normal incidence Mo/Si multilayer mirrors, led to the development of high resolution lithographic apparatuses operating in this sub-region [6, 7]. Consequently, EUV sources are largely studied and exploited for metrology and tests on EUV components: detectors, special optics, lithographic masks, photoresists and innovative materials.

Due to the EUV short penetration depth in almost every material [8], no lenses are available and EUV radiation propagates just in vacuum, or in really low residual gas pressure: 1 mbar of air totally absorbs EUV radiation on a few centimeters path and, for example, Xe gas is even more absorbing [8].

Excluding synchrotron machines or free electron lasers, plasma sources are needed to efficiently generate EUV radiation. As a first approximation (black–body), the plasma temperature T determines the radiation spectrum peak photon energy E_0: $E_0(\mathrm{eV}) \simeq 3 \cdot T(\mathrm{eV})$. Anyway, it must be emphasized that the line emission characteristics of the emitted spectrum depend on the nature of the material from which the plasma is generated and on the plasma heating method. For instance, EUV radiation peaked at $h\nu = 90\,\mathrm{eV}$ ($\lambda \simeq 13.8\,\mathrm{nm}$), requires $T \simeq 30\,\mathrm{eV} \equiv 3.5 \cdot 10^5\,\mathrm{K}$. Since, in practice, in the case of high density ($\simeq 10^{21}\,\mathrm{cm}^{-3}$) plasmas, that is needed to obtain a good EUV emission, this range of temperatures can be maintained in a small volume $V \simeq 1\,\mathrm{mm}^3$ just for a short time $\tau \simeq 100\,\mathrm{ns}$ [9-11], only pulsed EUV sources have been developed.

An EUV Xe-fed Discharge Produced Plasma (DPP) source is available and operating at the ENEA Frascati Laboratories. Its main features will be discussed in the following.

2. – The ENEA DPP EUV radiation source

The ENEA DPP EUV radiation source is fully operating and stit is suitable for applications in surface treatments, photonic materials processing, sub-micrometric patterning [6], etc.

The DPP has been designed following a cylindrical symmetry to minimize the parasitic inductance of the main discharge circuit [9]. In fig. 1 the schematic of the DPP electric circuit is reported as reference. The DPP is supplied by two electric discharges: an initial long pulse low-current pre-ionizing one, followed by the fast high-current main discharge, which leads to the high-temperature plasma formation [6, 9, 10, 12]. Briefly, the DPP working principle can be described as follows [6, 9, 10, 12]:

- a low pressure (0.5–1.5 mbar) Xe gas, filling an alumina tube (3 mm inner diameter, 7–13 mm length), is pre-ionized by the first discharge ($\simeq$30 A, $\simeq$20 μs);
- after a few μs delay with respect to the start of the pre-ionizing discharge, the low-inductance 50 nF glycol cylindrical capacitor, charged up to $\simeq$25 kV, produces the second discharge (12–13 kA peak current, 240 ns half period) in the pre-ionized gas through a triggered spark-gap;

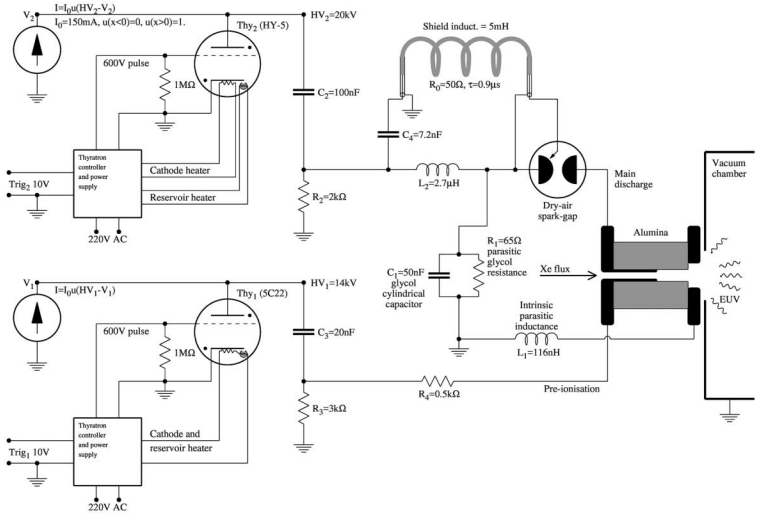

Fig. 1. – DPP electric circuit schematic.

- the resulting magnetic field (>1 T near the alumina tube at the current peak) pinches the plasma towards the tube axis;
- the plasma resistance rises, thus the plasma temperature can increase up to 30–40 eV;
- the hot plasma emits radiation before relaxing and cooling.

The DPP emits radiation on a broad spectral range including EUV, UV, visible light etc. The source is optimized to emit EUV pulses in the band [9, 10, 13]:

$$\begin{cases} h\nu \simeq 69\text{–}124 \text{ eV}, \\ \lambda \simeq 10\text{–}18 \text{ nm}. \end{cases}$$

It is typically Xe gas fed, but other gasses can be utilized to modify the characteristics of the emission.

To select the $\lambda = 10$–18 nm region, which is the Xe main emission EUV sub-band, a Zr filter must be used. The Zr exhibits a good EUV transmission in the $\lambda = 10$–18 nm range [8], well matching the DPP emission spectrum [13]. In fig. 2 a typical spectrum of the DPP EUV radiation is reported together with the transmission coefficient of a 150 nm thick Zr filter [8]. This Zr filter (by Luxel Corp.) transmits $\simeq$56% of the incident DPP EUV radiation.

In fig. 3 a typical time evolution of the high voltage V_1 on the glycol capacitor, of the main discharge current I_{cap} and of the EUV pulse, as detected by a 300 nm-Zr-filtered absolute PIN diode (IRD/Optodiode AXUV20HS1BNC) placed at 54 cm from plasma, 10° off-axis, is shown. This PIN diode configuration has been fixed during all measurements. The EUV emission is characterized by multiple pulses, corresponding to the discharge current oscillations, which produce subsequent less efficient plasma compressions.

Presently, the DPP emits more than 30 mJ/sr/shot in the $\lambda = 10$–18 nm wavelength region at 10 Hz repetition rate within $\simeq$0.9 sr solid angle, with a pulse to pulse stability

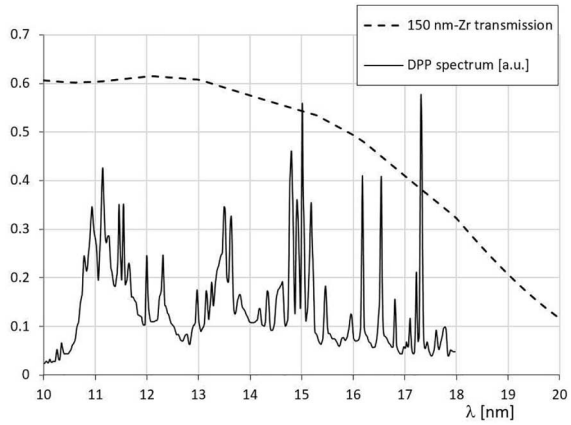

Fig. 2. – Spectrum of the DPP EUV emitted radiation and the transmission coefficient of a 150 nm thick Zr filter.

$\leq$3% r.m.s. The EUV pulses typical duration is $\simeq$100 ns FWHM [6], while the optical EUV source transverse size ϕ is less than 300 μm, a factor ten less than the initial diameter of the plasma [6, 10, 12].

The DPP is equipped with a vacuum chamber for the applications of the EUV radiation. At the moment, when the DPP is operating, in addition to a residual air pressure of $\simeq 10^{-5}$ mbar, a Xe gas pressure of $\simeq 10^{-2}$ mbar is present in the vacuum chamber, due to a dynamic equilibrium between the incoming Xe gas flux (5–25 sccm) and the available pumping speed. The implemented diagnostics and the reliable DPP performances allow various controlled applications like direct EUV exposures of materials with a minor damage from plasma debris bombardment [3, 4, 6].

Looking at the shape of the EUV pulse reported in fig. 3, it is possible to note a fast front edge at the starting of the first pulse, partially integrated by the 10-ns risetime

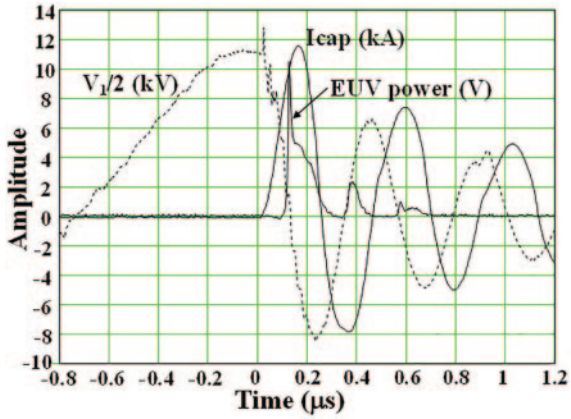

Fig. 3. – Temporal evolution of the high voltage V_1 on the glycol capacitor, of the main discharge current $I_{\rm cap}$ and of the EUV pulse as detected by a 300 nm-Zr-filtered absolute PIN diode placed at 54 cm from plasma and 10° off-axis.

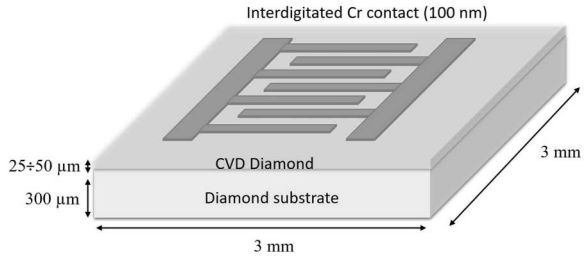

Fig. 4. – IEC diamond detector schematic.

of the used silicon PIN diode. This overshooting indicates that the plasma column has reached its maximum heating and radial compression and that, by few ns, the kinetic energy collected by the collapsing plasma cylindrical shock wave is converted into thermal energy [9, 11]. To better analyze this phenomenon, a faster EUV detector is needed. In the following we will discuss the measurements of the DPP emission by using the above-mentioned fast response diamond detectors.

3. – The diamond detectors

At URTV, two different types of diamond detectors have been developed. The Sandwich Configuration (SC) detectors [1, 14] will not be treated in this work, whereas the Interdigitated Electrode Configuration (IEC) detectors [1, 15, 16] have been used during our measurements and will be discussed in the following.

In fig. 4 a schematic of a IEC detector is shown, while the image of a utilized IEC detector obtained with a 2.5× optical microscope is reported in fig. 5, where the layout of the two comb-shaped interdigitated electrodes is evident.

In short, an IEC detector consists of a high-purity synthetic intrinsic single-crystal diamond (25–50 μm thick) grown by microwave enhanced plasma Chemical Vapor Deposition (CVD), on a commercial low-cost High Pressure High Temperature (HPHT) diamond substrate (overall typical size: $3\text{–}4 \times 3\text{–}4 \times 0.3\text{–}0.5\,\mathrm{mm}^3$). On the CVD diamond surface, two interdigitated comb-shaped Cr electrodes, positioned as shown in figs. 4 and 5, are fabricated by photolithography. The Cr coating is typically 100–150 nm thick.

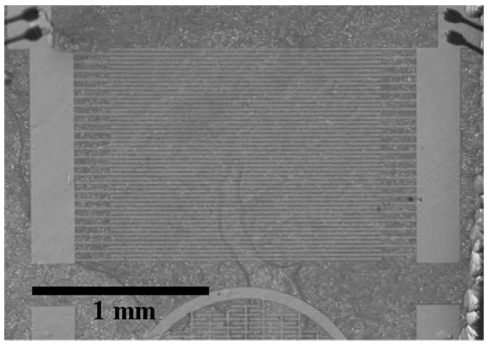

Fig. 5. – Image of the (5-20) IEC diamond detector obtained with a 2.5× optical microscope.

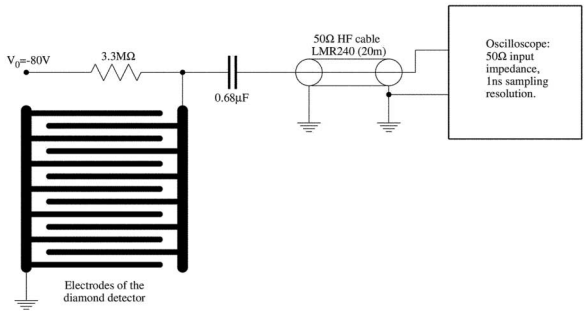

Fig. 6. – IEC diamond detector bias circuit schematic.

The width of each comb tooth and each gap between two adjacent electrode elements is in the range 5–25 μm. The nominal width of the tooths (θ) and the nominal value of the gaps (γ), both expressed in μm, characterize a specific detector and its name as ($\theta - \gamma$). For instance, fig. 5 refers to a (5-20) IEC detector. In our measurements we used three IEC detectors: (5-5), (10-10) and (5-20).

The band-gap of intrinsic diamond is: $E_{\mathrm{gap}} \simeq 5.5\,\mathrm{eV}$. Therefore, energetic enough photons ($h\nu > E_{\mathrm{gap}}$) impinging on the CVD diamond surface and penetrating in the material, can generate electron-hole pairs, theoretically free to travel into the whole crystal. However, in absence of a driving electric field, the pairs quickly recombine. On the contrary, if a bias voltage is applied to the electrodes, the electrons and the holes move in opposite directions. If they reach the electrodes, an electrical signal is generated. The intensity of the collected current is then proportional to the amount of photons per second, *i.e.*, to the intensity of the radiation. The current signal is converted into a voltage one by the 50-ohm input impedance of a high frequency oscilloscope. The high mobility of the charge carriers and the low dielectric constant of diamond ($\varepsilon_{\mathrm{r}} \simeq 5.7$) allow obtaining very low risetime (0.1–1 ns) detectors. The DPP EUV radiation has a penetration depth in diamond of $\simeq$0.1–0.2 μm [8], where the electric field generated by the bias voltage is certainly present, given the values of γ. The IEC detectors seem to be a very good choice to characterize the temporal evolution of the DPP emission.

4. – IEC diamond detectors and the DPP EUV radiation

In fig. 6 we report the schematic of the IEC detector bias circuit. This simple circuit allows obtaining a positive signal with negligible distortion. The decoupling capacitor is large enough to avoid distortions of the signal at the frequencies of our interest, as long as the amplitude of the signal remains well below the absolute value of the bias voltage. This capacitor works both as DC decoupling as well as power supply of the detector during the EUV pulse. The LMR240 coaxial 50-ohm cable exhibits an attenuation of $\simeq$27 dB at 1 GHz (for 100 m cable)([1]). The used oscilloscope (an old 1 GHz Techtronix DSA 602) can work at 1 ns effective sampling rate.

As already mentioned, to select the $\lambda = 10$–18 nm EUV band we filtered the DPP emitted radiation by using a 150 nm thick Zr filter placed in front of the detectors. The three tested diamond detectors have been positioned, one at time, in front of the

([1]) As a comparison, in the case of the commonly used RG58-C/U this value is $\simeq$60 dB.

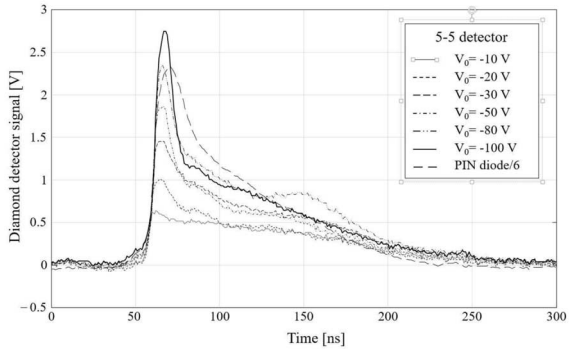

Fig. 7. – (5-5) IEC diamond detector signal for different bias voltages. The detector, with the Zr filter, was at 43 cm from plasma. The signal of the PIN diode is reported as reference.

DPP plasma in the vacuum chamber, on the optical axis of the system. In order tobe able to compare the signals of different detectors, obtained during different DPP shots, the diamond detector signals have been normalized to the corresponding PIN diode amplitude.

We studied the response of the IEC detectors for different values of V_0 and determined the best detector to be exploited to detect the DPP EUV emission. As an example, in fig. 7 the signal of the (5-5) IEC detector is reported for various values of the bias voltage V_0. The higher the $|V_0|$, the larger the signal of the IEC detector. Moreover, the shape of the signal depends on V_0. In particular, the amplitude of the fast EUV initial peak depends on V_0 in a stronger way than that of the slow components of the EUV pulse. To correctly calibrate this kind of detectors, V_0 must be carefully chosen. To avoid possible detector damages, $V_0 = -80\,\mathrm{V}$ has been chosen as a good compromise for the working point.

In fig. 8 the signals of the three tested (5-5, 10-10 and 5-20) detectors are reported for $V_0 = -80\,\mathrm{V}$. Since the effective sensible area of IEC detectors [1] is a narrow ($\simeq$5–10 μm) region around the anode, the response of the three detectors resulted quite similar one to each other. Based on various measurements, the (10-10) detector proved to be the most stable and reliable.

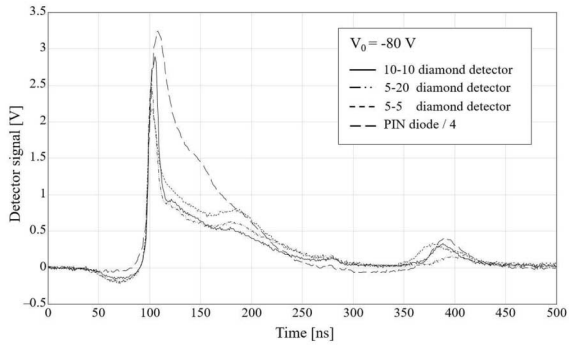

Fig. 8. – Comparison of the tested IEC detectors (5-5, 10-10 and 5-20). The detectors, with the Zr filter, were at 43 cm from plasma. The signal of the PIN diode is reported as reference.

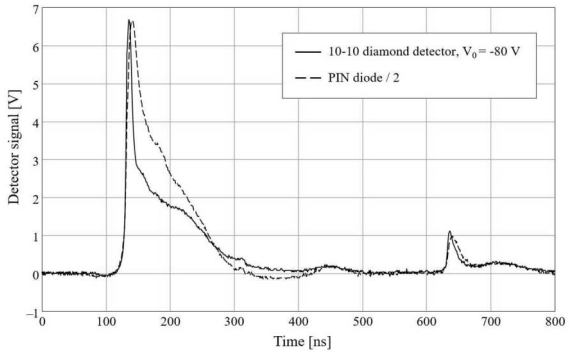

Fig. 9. – Comparison between the (10-10) IEC diamond detector signal and that of the PIN diode. The diamond detector, with the Zr filter, was at 30.5 cm from plasma.

In fig. 9 a comparison between the (10-10) IEC diamond detector signal and that of the PIN diode is reported. In this case, the diamond detector was placed nearer to the plasma, to improve the signal to noise ratio. The EUV fast peak ($\simeq$8 ns FWHM), corresponding to the plasma transverse collapse and to the maximum plasma heating, is now evident.

Removing the Zr filter from the (10-10) IEC detector, we exposed the detector to the total band of the DPP emission. In fig. 10 the obtained signal is shown. By comparing fig. 10 with fig. 9 and taking into account the doubled EUV components, due to the absence of the Zr filter, one can estimate that the energy emitted in the $\lambda = 10$–18 nm is similar to that emitted in the UV region, down to E_{gap}. The plasma UV emission is longer than the EUV one and it does not vanish when the discharge current inverts its direction, because the plasma temperature remains high enough for the UV emission.

Even if the energy related to the fast initial EUV peak is a small fraction of the total energy of the EUV pulse, the formation of the fast peak indicates that the plasma is reaching its maximum heating [11]. Plasma dynamics also depends on the Xe gas initial average pressure p_{i} in the alumina tube. The value of p_{i} [9] depends on the Xe

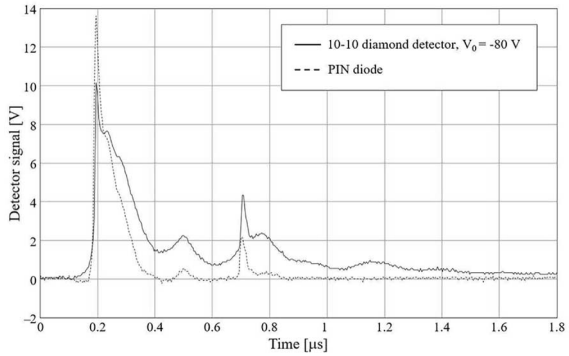

Fig. 10. – EUV + UV DPP emission obtained by the (10-10) IEC diamond detector, without Zr filter, placed at 30.5 cm from plasma. The signal of the PIN diode is reported as reference.

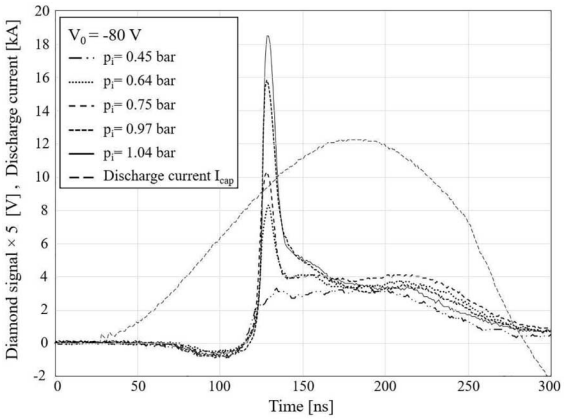

Fig. 11. – EUV emission *vs.* initial Xe gas pressure p_{i} in the alumina tube, as detected by the (10-10) IEC detector, with the Zr filter, placed at 43 cm from plasma. The main discharge current is reported as reference.

gas inlet flux. This flux, in turn, depends on the Xe gas pressure p_{u} upstream from a 50 μm diameter nozzle. In fig. 11 the (10-10) IEC detector signal for different p_{i} values is reported. To obtain the plasma fast transverse collapse and the cylindrical shock wave kinetic thermal contribution [11], that generates the fast EUV peak, the initial Xe gas pressure, *i.e.*, its initial density, must be high enough. Further analysis and experiments on this plasma behaviour are planned.

5. – Conclusions

A DPP EUV source is operating at ENEA. It is suitable for various applications. Recently, in addition to the already performed DPP characterizations, IEC diamond detectors, developed and fabricated at URTV, have been utilized. Three IEC diamond detectors (5-5, 10-10 and 5-20) have been tested and calibrated in the DPP EUV emission spectral range. Thanks to the high speed response of these detectors, the fast EUV peak ($\simeq$8 ns FWHM), that occurs in correspondence with the plasma collapse and the plasma maximum heating, has been better characterized than when using silicon PIN diodes. By varying the initial Xe gas average pressure in the alumina tube, we observed that, to obtain the plasma fast transverse collapse with the cylindrical shock wave kinetic thermal contribution, the initial Xe gas density must be high enough.

Further experiments are planned both on the plasma dynamics and on diamond detector characterizations.

REFERENCES

[1] Verona C. *et al.*, *JINST*, **15** (2020) C09066.
[2] Attwood D., *Soft X-Rays and Extreme Ultraviolet Radiation Principles and Applications* (Cambridge University Press) 2007.
[3] Torti E. *et al.*, *ChemPhotoChem*, **2** (2018) 425.
[4] Botti S. *et al.*, *ACS Appl. Electron. Mater.*, **1** (2019) 2560.
[5] Baldacchini G. *et al.*, *Rev. Sci. Instrum.*, **76** (2005) 113104.

[6] Mezi L. *et al.*, *Proc. SPIE*, **11042** (2019) 110420Z.
[7] Bollanti S. *et al.*, *EPL*, **84** (2008) 58003.
[8] Henke B. L. *et al.*, *At. Data Nucl. Data Tables*, **54** (1993) 181, http://henke.lbl.gov/optical_constants.
[9] Mezi L. and Flora F., *La sorgente DPP di radiazione nell'estremo ultravioletto a scarica elettrica in gas rarefatto: principi fisici, caratterizzazione ed ottimizzazione*, ENEA Technical Report RT/2012/15/ENEA, https://iris.enea.it/handle/20.500.12079/61122.
[10] Mezi L. *et al.*, *PoS*, **ECPD2015** (2015) 125.
[11] Koshelev K. N. *et al.*, *Radiative collapse in Z-pinches*, in *EUV Sources for Lithography*, edited by Bakshi V., (SPIE Press, Bellingham, WA) 2006, Chapt. 6, https://doi.org/10.1117/3.613774.ch6.
[12] Bollanti S. *et al.*, *High Power Laser Sci. Eng.*, **3** (2015) e29.
[13] Zuppella P. *et al.*, *Plasma Sources Sci. Technol.*, **18** (2009) 025014.
[14] Cesaroni S. *et al.*, *Fusion Eng. Design*, **166** (2021) 112323.
[15] Balducci A. *et al.*, *Appl. Phys. Lett.*, **86** (2005) 193509.
[16] Forneris J. *et al.*, *EPL*, **108** (2014) 18001.